

Stress Analysis of Elastic–Plastic Contact Damage in Ceramic Coatings on Metal Substrates

Anthony C. Fischer-Cripps,^{*†} Brian R. Lawn,^{*} Antonia Pajares,^{*‡} Lanhua Wei^{*§}

Materials Science and Engineering Laboratory, National Institute of Standards and Technology,
Gaithersburg, Maryland 20899

An elastic–plastic analysis of damage in ceramic coatings on metal substrates from contacts with spherical indenters is made using finite element modeling. Computations are carried out specifically for plasma-sprayed alumina:titania on a soft steel. The algorithm assumes an elastic sphere with frictionless contact on a flat elastic–plastic layered specimen, and incrementally evaluates the expanding contact field as a function of applied load. Two key aspects of the contact field are examined: (i) the indentation stress–strain curve; (ii) the damage zone geometry. Composite coating/substrate indentation stress–strain curves are computed for two coating thicknesses, using input material parameters from iterative fits to data from control tests on free-standing coating and substrate materials. Contours of principal shear stresses, most notably those contours corresponding to yield zone boundaries in both the softer substrate and the harder coating, are mapped out in the fully plastic region. Corresponding distributions of tensile stresses are also mapped out, and are shown to correlate with the locations of transverse fractures in the coating. General implications concerning material and geometrical design of ceramic-based layer structures are discussed.

I. Introduction

THE failure of ceramic coatings on metal substrates, from plasma spraying or other deposition methods, is an important practical problem.^{1–7} Stress states and damage modes in such layer structures are not well understood, especially when there is accompanying plastic deformation. Plasticity can be an especially important factor in interfacial coating/substrate delamination and through-thickness coating failures in cycling loading, from strong augmentation of interlayer mismatch stresses. Accordingly, there is a need for methodologies to analyze stresses in brittle coatings on soft substrates, with due provision for nonlinear components in the intrinsic stress–strain responses.

Elastic–plastic mismatch effects in layer structures are most conspicuously demonstrated in contact testing, where uncommonly high stress concentrations can produce extensive yield in the soft components.⁷ Of all contact test configurations, perhaps the most enduring is that in which a hard sphere is pressed onto a flat specimen surface—so-called Hertzian indentation.

Hertzian indentation has been used for over a century in the analysis of bulk homogeneous materials,⁸ as a probe of plasticity in soft materials like metals and polymers^{9–11} and cone fracture in ideally brittle solids like glasses and fine-grain ceramics.^{8,12–15} Recently, Hertzian indentation has been applied to tough ceramic systems with heterogeneous microstructures (coarse grains, weak grain or interphase boundaries, high internal stresses), where an intermediate form of damage is observed.¹⁶ This damage is termed “quasi-plastic” or “quasi-ductile” because it has the outward macroscopic appearance of conventional indentation plasticity, and is shear-driven; it is nevertheless also fundamentally different from conventional plasticity, in that the basic microscopic unit of slip is not classical dislocation motion but some constrained intra- or intergrain planar weakness^{17–22} (“shear fault,” analogous to a closed microcrack²³). In the context of layer structures, such quasi-plastic modes raise the possibility of attendant, if limited, yield in otherwise brittle components.^{24–26}

Consequent extension of Hertzian testing to the investigation of damage modes in plasma-sprayed ceramic coatings on metal substrates confirms the role of pervasive yield in the damage response.^{7,27,28} For a relatively hard alumina–titania coating on a soft steel substrate the indentation stress–strain curve closely follows that of the bulk coating material at low contact load, and tends asymptotically to that of the bulk substrate material at high load, with an intervening maximum.²⁷ Such a stress–strain curve attests to the exceptional damage tolerance of certain ceramic coating systems. Subsurface sections confirm the deformation to be wholly elastic in the low-strain region, becoming partially plastic in the intermediate region of the stress maximum as the substrate begins to yield, and ultimately fully plastic in the high-strain region as extensive yield in the substrate and limited yield in the coating begin to dominate the deformation. Through-thickness cracks may develop in the coating, predominantly during the loading, and delamination cracks during the unloading, depending on the thickness and microstructural defect content in the coating.^{7,27,28} These observations point to a complex interplay between elastic, plastic, and fracture processes in ceramic/metal systems.²⁹

The first step in modeling contact damage in interlayer structures is an analysis of the stress field, with due allowance for nonlinearity in both layers. Any such stress analysis poses considerable theoretical challenges, and appears to be beyond analytical solution. Here we resort to numerical methods, using finite element modeling (FEM). Elastic–plastic analyses of Hertzian-like contact deformation in coating/substrate systems by FEM have been conducted by others,^{3,30} but on hypothetical material systems, leaving the facility of FEM to shed light on the nature and scale of observed damage modes in real material systems to be confirmed. Such a facility is foreshadowed in a more recent FEM study of Hertzian contact damage in bulk heterogeneous ceramics,³¹ with an appropriate “calibration” of input elastic and plastic parameters into a simple nonlinear stress–strain constitutive function, we are able to reproduce all the essential features of the indentation stress–strain curves and the quasi-plastic zone geometry observed in those materials. Recognizing the singular capacity of FEM protocols to handle

M. Thouless—contributing editor

Manuscript No. 192097. Received January 1, 1996; approved March 26, 1996.

Supported by the U.S. Air Force Office of Scientific Research and the Ministerio de Educación y Ciencia (DGICYT), Spain.

^{*}Member, American Ceramic Society.

[†]Guest scientist from the Department of Materials Science and Engineering, Lehigh University, Bethlehem, Pennsylvania 18015. Now in the Department of Applied Physics, University of Technology at Sydney, Sydney, NSW 2007, Australia.

[‡]Guest scientist from the Departamento de Física, Universidad de Extremadura, 06071 Badajoz, Spain.

[§]Guest scientist from the Department of Physics and Astronomy, Wayne State University, Detroit, Michigan 48201. Now at ThermoWave, Fremont, California 94539.

extra degrees of configurational complexity with no more than minor inconvenience, progression to a coating/substrate structure would appear to require no more than a simple extension of the parametric calibration from one to two material components.

Accordingly, the aim of the present study is to conduct a stress analysis of Hertzian contact on ceramic/metal layer structures using the above FEM code³¹ as a theoretical complement to experimental observations of damage modes. For an illustrative case study, we consider the plasma-sprayed alumina:titania/steel system described in one of our earlier experimental studies.²⁷ Calibration tests on the constituent alumina:titania coating and soft steel substrate materials provide necessary input data for the computations. We demonstrate how FEM can reproduce the critical observed features of the composite coating/substrate stress-strain curve and plastic zone geometry. With these critical features verified, we evaluate the tensile stress distributions in the coating, and thereby establish a basis for prospective fracture mechanics analysis of observed crack patterns. Finally, implications of the study in the context of design of ceramic/metal interlayer structures are briefly discussed.

II. Contact Damage in Coating/Substrate Systems

In this section we summarize essential evidence for contact damage in plasma-sprayed alumina:titania (Al_2O_3 :40 wt% TiO_2) coatings on steel, with thicknesses relevant to thermal barrier coatings. We choose this system because the interlayer elastic-plastic mismatch is large, and because pertinent experimental contact data are available from previous studies.²⁷ At the same time, we emphasize the generality of our approach to other layer structures with ceramic components.

Relevant details of the Al_2O_3 :40 wt% TiO_2 system are as follows.²⁷ Coatings are air plasma sprayed directly onto grit-blasted soft steel substrates ≈ 3 mm thick. Coating thicknesses are nominally $d = 160 \mu\text{m}$ ("thin") and $470 \mu\text{m}$ ("thick"), but subject to variations of up to 10% point-to-point within any given specimen and 20% specimen-to-specimen. Control free-standing "bulk" specimens of the Al_2O_3 :40 wt% TiO_2 coating and steel substrate materials are also prepared, to ≈ 5 mm thickness. Coating porosity is estimated at $\approx 4\%$. Exploratory Vickers indentations confirm that the hardness of the coating

(5.0 ± 0.6 GPa) is greater than that of the substrate (1.2 ± 0.1 GPa) (although the reverse is true for Young's modulus—see Table I, later).

Hertzian contact tests are performed on polished top surfaces of the coating/substrate specimens using tungsten carbide (WC) spheres of radius $r = 3.18$ mm, up to peak loads $P = 1500$ N.²⁷ Indentation stress-strain data are obtained by measuring the residual contact radius a at each load P , and then computing indentation stress $p_0 = P/\pi a^2$ as a function of indentation strain a/r .^{9,17,32,33} Data points for the two Al_2O_3 :40 wt% TiO_2 /steel layer composites are plotted in Fig. 1.²⁷ These data are subject to experimental errors $\approx 10\%$ in p_0 and $\approx 5\%$ in a/r , from $\approx 5\%$ uncertainty in the measurement of a . Analogous stress-strain data are obtained for the free-standing Al_2O_3 :40 wt% TiO_2 and steel specimens (although over a wider range of sphere radius, to expand the data range), for subsequent parametric calibration (Section III). (The data for Al_2O_3 :40 wt% TiO_2 fall considerably below comparative data for dense alumina¹⁷ or zirconia,³⁴ consistent with a high pore and defect content.) The solid curves are theoretical fits to be described later (Section IV). Note the uncommonly high stress levels achieved in these tests, in the gigapascal range.

The departures from linear elasticity in the data for the free-standing coating as well as the substrate at higher stress levels in Fig. 1 indicate the presence of yield in both materials.^{17,31-33} The responses for the composite coating/substrate systems follow the coating curve at low strains, and tend asymptotically to the substrate curve at high strains, with an intervening stress maximum. The very existence of this stress maximum is contingent on the coating remaining significantly harder than the substrate,⁷ and its value diminishes as the coating becomes thinner relative to the sphere radius.

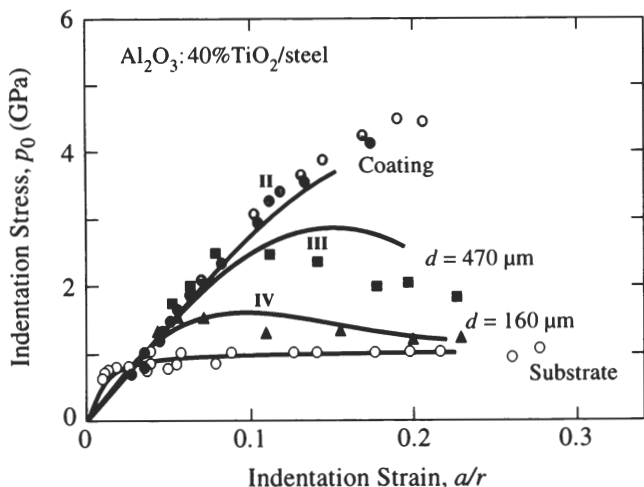


Fig. 1. Indentation stress-strain curve for plasma-sprayed Al_2O_3 :40 wt% TiO_2 coatings on steel. Data points are experimental tests (Section II): free-standing coating and substrate, sphere radii $r = 1.98$ to 12.7 mm (not distinguished here); composite coating/substrate system, sphere radius $r = 3.18$ mm, coating thicknesses $d = 160$ and $470 \mu\text{m}$. Solid curves are FEM data fits (Section IV). Note maximum in curve for each composite coating/substrate system. Points II, III, and IV correspond to micrographs in Figs. 2, 3, and 4, respectively. (Data from Ref. 27.)

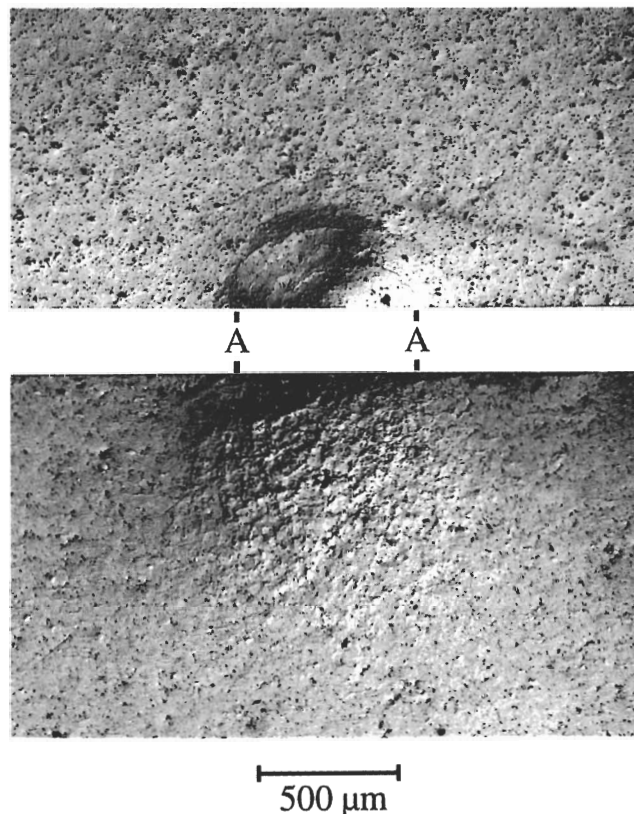


Fig. 2. Contact damage in free-standing plasma-sprayed Al_2O_3 :40 wt% TiO_2 material. Indentation with WC sphere, radius $r = 3.18$ mm, load $P = 1000$ N, bonded-interface specimen, contact diameter AA. Half-surface view (upper), showing surface impression with ring cracks; section view (lower), showing constricted yield (quasi-plastic) zone beneath contact. Optical micrographs, Nomarski illumination. (From Ref. 27.)

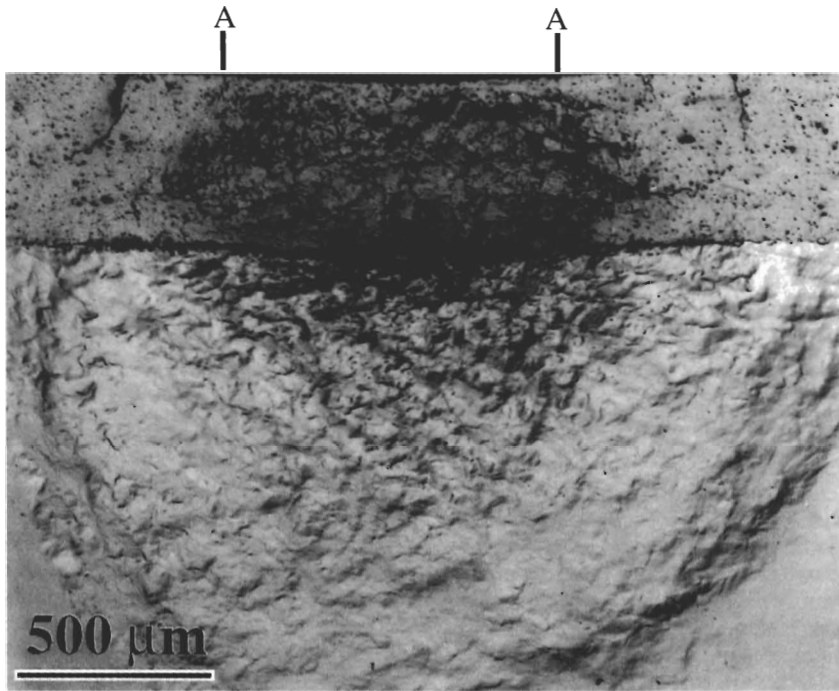


Fig. 3. Contact damage in Al_2O_3 :40 wt% TiO_2 /steel system, coating thickness $d = 470 \mu\text{m}$ ("thick" coating). Indentation with WC sphere, radius $r = 3.18 \text{ mm}$, load $P = 1500 \text{ N}$, bonded-interface specimen, contact diameter AA. Section view, showing extensive yield zone in substrate, limited yield plus fracture in coating. Optical micrograph, Nomarski illumination. (From Ref. 27.)

Micrographs of contact yield zones obtained using WC spheres of radius $r = 3.18 \text{ mm}$ on "bonded-interface" specimens are shown in Figs. 2–4.^{7,27} These micrographs represent load states well within the full plasticity region of the respective stress-strain curves (see appropriately marked points **II**, **III**, and **IV** in Fig. 1). For the free-standing Al_2O_3 :40 wt% TiO_2 (Fig. 2), quasi-plastic deformation is apparent as a residual impression in the half-surface view, and as a confined droplike zone immediately beneath the contact in the section view, typical of bulk heterogeneous ceramics.³¹ For both the thick (Fig. 3) and thin (Fig. 4) Al_2O_3 :40 wt% TiO_2 coating composites, plasticity is extensive in the soft steel substrate. Limited quasi-plasticity in the Al_2O_3 :40 wt% TiO_2 is also discernible below the contact, more so at the higher load indentation in the thicker coating; note the relatively deep residual impressions within the contact, again more prominent in the thicker coating. These observations, in conjunction with the nonlinear stress-strain curves, foreshadow a pervasive component of shear stress in an otherwise hydrostatic compression contact field.³¹

Cracking is also distinctly evident in the micrographs.²⁷ In the free-standing Al_2O_3 :40 wt% TiO_2 (Fig. 2), surface ring cracks are observed in the half-surface view, but these do not penetrate to any perceptible depth in the section view. This suppression of subsurface fracture is another characteristic of bulk heterogeneous ceramics.^{25,31} In the coating configurations (Figs. 3 and 4), on the other hand, the ring cracks outside the contact penetrate much deeper below the surface. A second set of fine transverse cracks forms at the coating/substrate interface immediately below the contact and propagates upward into the coating. These two sets of transverse cracks extend predominantly during the loading, in a highly stable manner, and do not fully traverse the coating until extreme loads are achieved. Finally, delamination cracks form at the coating/substrate interface, toward the very end of the unloading half-cycle. The presence of these various cracks in the layer structures signifies the enhancement of tensile stresses from a "plate bending" component in the contact field.²⁷

III. Finite Element Modeling

A commercial package (Strand, G&D Computing, Sydney, Australia) is used to carry out finite element modeling (FEM)

of the indentation configurations described in Section II.³¹ Our specific algorithm models an indenting sphere, radius $r = 3.18 \text{ mm}$, in frictionless axisymmetric contact with an initially flat layer specimen, coating thicknesses $d = 160$ and $470 \mu\text{m}$. The cross-section mesh, part of which is shown in Fig. 5, consists of axisymmetric quadrilateral plate elements, with the highest density of cells close to the contact, over a half-space $4 \text{ mm} \times 4 \text{ mm} \times 4 \text{ mm}$. Contact is incremented in 30 steps, from initial contact to a peak load $P = 1500 \text{ N}$, with a maximum 50 iterations per increment to allow for convergence to

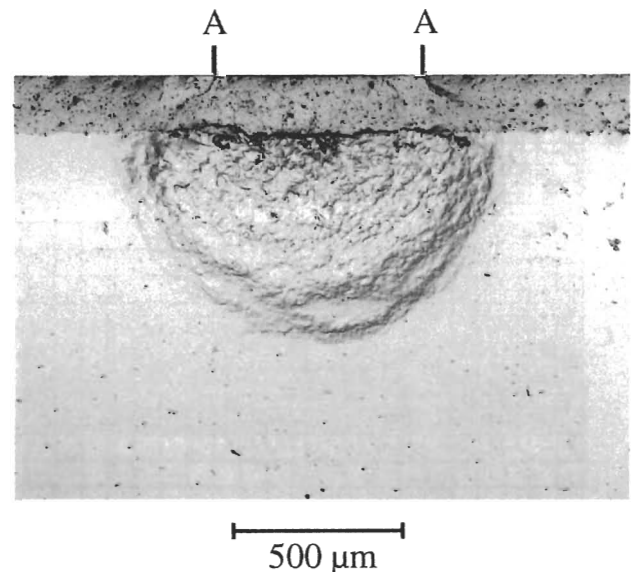


Fig. 4. Contact damage in Al_2O_3 :40 wt% TiO_2 /steel system, coating thickness $d = 160 \mu\text{m}$ ("thin" coating). Indentation with WC sphere, radius $r = 3.18 \text{ mm}$, load $P = 500 \text{ N}$, bonded-interface specimen, contact diameter AA. Section view, showing extensive yield zone in substrate, and coating fracture. Optical micrograph, Nomarski illumination. (From Ref. 27.)

equilibrium. This convergence is achieved with a force tolerance of better than 0.1% and displacement tolerance 0.5%. At the end of each load increment the contact radius a is evaluated, from which the stress-strain quantities $p_0 = P/\pi a^2$ and a/r are calculated. It is assumed that the coating remains bonded to the substrate across the interface during the loading (recall that delamination occurs only during unloading).

The algorithm has general provision for input of constitutive uniaxial elastic-plastic stress-strain responses $\sigma(\epsilon)$ for the two layer materials, and for the indenter. In our calculations we allow each material to deform according to a (three-dimensional) critical shear stress condition with linear strain-hardening.³¹

$$\sigma = E\epsilon \quad (\sigma < Y) \quad (1a)$$

$$\sigma = Y + \alpha(\epsilon E - Y) \quad (\sigma > Y) \quad (1b)$$

with E Young's modulus, Y the uniaxial stress for the onset of yield, and α a dimensionless strain-hardening coefficient in the range $0 \leq \alpha \leq 1$ ($\alpha = 1$, fully elastic; $\alpha = 0$, fully plastic). Whereas the assumption of fully plastic behavior is often adequate for soft metals, the same is generally not true for ceramics.³¹ Nor is the assumption of fully elastic behavior always guaranteed for the indenter material,³¹ although in the layer materials under consideration here the elastic limit of the WC is never exceeded.

In general, there will be superposed macroscopic residual stresses in the coating from thermal expansion mismatch with the substrate. We ignore consideration of any such stresses here, noting that Vickers radial crack patterns on representative coating sections show no signs of pronounced anisotropy in our material system.²⁷ We also ignore explicit consideration of the postcontact residual field that inevitably drives the coating/substrate delamination, for lack of provision in the current algorithm to accommodate unloading.

IV. Results

We begin the FEM analysis by attempting to account for the essential features of the indentation stress-strain curves for the coating/substrate structures in Fig. 1. The first step is to match the material parameters in Eq. (1) to the control stress-strain data for the bulk Al_2O_3 :40 wt% TiO_2 coating and steel substrate. (An analogous computational match for the WC indenter

material is available from a preceding study.³¹) For each material, Young's modulus E is predetermined from the slopes of appropriate stress-strain curves in the initial linear region, and yield stress Y from the critical loads at first observable subsurface damage in sectioned specimens.²⁷ The strain-hardening parameter α is adjusted to provide a best fit to each data set. Table 1 lists these calibrated parameters. The solid curves in Fig. 1 through the Al_2O_3 :40 wt% TiO_2 and steel data are the corresponding smoothed-out FEM stress-strain functions.³¹ These curves are estimated to be subject to a computational variability of $\approx 3\%$ in the contact radius (from convergence and grid-size errors), resulting in uncertainties of $\approx 6\%$ in stress and $\approx 3\%$ in strain. Note that a value of α less than unity but greater than zero is needed to fit the Al_2O_3 :40 wt% TiO_2 data, confirming the existence of quasi-plasticity but with a significant strain-hardening coefficient.³⁵

Given these component calibrations, one may then carry out *a priori* calculations for the composite layer structures. It is necessary only to specify the coating thickness d , and to reassign material parameters within the subdivided coating and substrate layers. Again, the ensuing FEM stress-strain $p_0(a/r)$ functions for the two coating thicknesses are plotted as solid curves in Fig. 1. We see that the predictions are able to account for the qualitative features of the data, notably the initial rise closely parallel to the coating curve and the ultimate asymptotic tendency toward the substrate curve, with intervening maximum. On the other hand, even allowing for the previously cited uncertainty bounds (computational, $\approx 6\%$ stress and $\approx 3\%$ strain; experimental, $\approx 10\%$ stress and $\approx 5\%$ strain), quantitative agreement is open to some question, particularly in the tail region for the thicker coating. Relaxation effects in the yield process from stable crack propagation in the coating layer, resulting in premature transfer of the contact stresses to the underlying substrate, may account in part for this apparent systematic discrepancy.

If we accept the computed stress-strain curves as adequately representative of the stress-strain data, the FEM algorithm may be used to map out the operative stress fields that drive yield and fracture in both coating and substrate.³¹ From evaluations of principal normal stresses σ_1 , σ_2 , and σ_3 ($\sigma_1 \geq \sigma_2 \geq \sigma_3$ everywhere except in the free-surface region, where $\sigma_2 < \sigma_3 = 0$),³¹ we plot the following stress contours in Figs. 6–8, corresponding to the contact load conditions in the micrographs of Figs. 2–4:

(i) In the upper diagrams, greatest principal shear stress, $\tau = \frac{1}{2}(\sigma_3 - \sigma_1)$ (except $\tau = \frac{1}{2}(\sigma_1 - \sigma_2)$ in the near-free-surface region³¹). Shading in these diagrams indicates the yield zones $\tau > \frac{1}{2}Y$ (graded in the ceramic component to indicate stress buildup from linear strain-hardening), for comparison with the observed yield zones. General features of the observed yield geometry are confirmed. For the free-standing Al_2O_3 :40 wt% TiO_2 , the computed yield contour (Fig. 6) reproduces the characteristic constriction in the damage zone immediately below the contact visible in the corresponding micrograph (Fig. 2).³¹ For the layer structures, most obvious is the extensive plastic zone in the substrate (Figs. 7 and 8), verifying the dominant role of substrate yield in the fully plastic region (Figs. 3 and 4). The prediction of limited yield in the coating is also consistent with observation, especially in the thicker coating (cf. Figs. 7 and 3). At the same time, there is again some question as to quantitative agreement: in the free-standing coating the predicted yield zone size relative to the contact diameter is somewhat smaller than observed; conversely, in the steel substrates in the layer structures the predicted sizes are somewhat larger than observed.

(ii) In the lower diagrams, greatest normal stress, σ_1 . Graded shading in these diagrams indicates regions of tension, $\sigma_1 > 0$. For the free-standing Al_2O_3 :40 wt% TiO_2 , the computed tensile field concentrates in shallow contours outside the contact (Fig. 6), with very modest magnitudes.³¹ Such stresses are apparently insufficient to drive surface ring cracks into the subsurface in this material (Fig. 2). For the layer structures

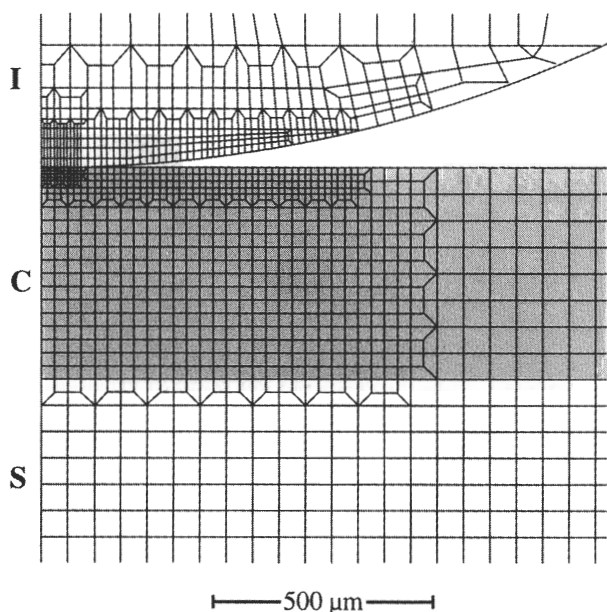


Fig. 5. FEM mesh for spherical indenter I on layer composite, coating C (shaded) on substrate S. Half-section view, near-contact region.

Table I. Constitutive Stress-Strain Data for Bulk Coating (Al₂O₃:40 wt% TiO₂), Substrate (Steel), and Indenter (WC) Materials*

	<i>E</i> (GPa)	ν	<i>Y</i> (GPa)	α
Al ₂ O ₃ :40 wt% TiO ₂	70 ± 4	0.26	2.1	0.75
Soft steel	210 ± 36	0.30	0.39	0
WC	614	0.22	6.0	0.10

*Young's modulus *E*, derived from slope of stress-strain curves for free-standing materials; Poisson's ratio ν , estimated from literature values; yield stress *Y*, evaluated from critical loads for onset of plastic deformation; strain-hardening coefficient α , evaluated from best fit to stress-strain data in full plasticity region.

(Figs. 7 and 8), the tensile field develops a second region of concentrated contours, at the lower bottom surface of the impressed coating, and builds up substantially in both tensile regions. One may usefully regard the coating as a flexural plate,²⁷ supported strongly at its edges by the elastic material beyond the contact circle but weakly beneath by the soft substrate. There is a strong gradation from tension to compression through the plate thickness, typical of contact fields.¹⁴ These regions of enhanced but confined tension correlate with the locations and sizes of the arrested through-thickness coating fractures observed in the corresponding micrographs (Figs. 3 and 4).

V. Discussion

The present study illustrates the potential value of FEM as a basis for analyzing complex elastic-plastic contact deformation

in mismatched layer structures. The FEM procedure, if somewhat restricted in its capacity to determine explicit functional dependencies on layer dimensions or material parameters, is nevertheless ideally suited to dealing with otherwise intractable stress field problems of this kind. Given appropriate constitutive relations for each of the material components (including the indenter), we can iteratively predict the contact response of any combined coating/substrate system. Calibration of the parameters in the input constitutive relations is effected by matching computed indentation stress-strain curves to appropriate experimental data from control tests on the individual material components. With this calibration, one can predict the stress-strain curves and yield zone geometries for specified composite coating/substrate structures. In our present study of Hertzian contact on the Al₂O₃:40 wt% TiO₂/steel ceramic/metal system, the predictions account for all the major qualitative features of the experimental observations. Quantitative agreement is

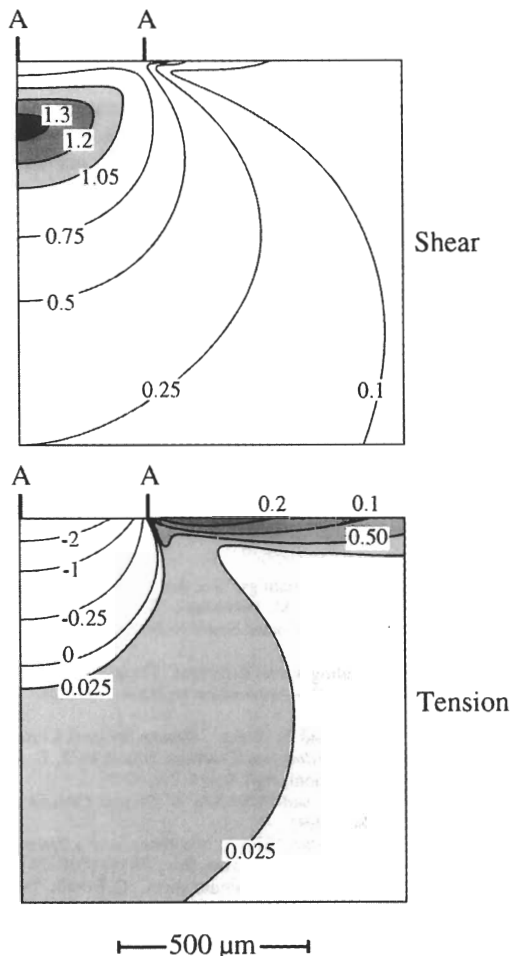


Fig. 6. FEM-computed stress contours for free-standing plasma-sprayed Al₂O₃:40 wt% TiO₂. Indentation with WC sphere, radius *r* = 3.18 mm, load *P* = 1000 N, contact radius AA (cf. Fig. 2). Upper diagram, maximum principal shear stresses, yield zone shaded; lower diagram, maximum principal stresses, tensile zone shaded. Stresses in gigapascals.

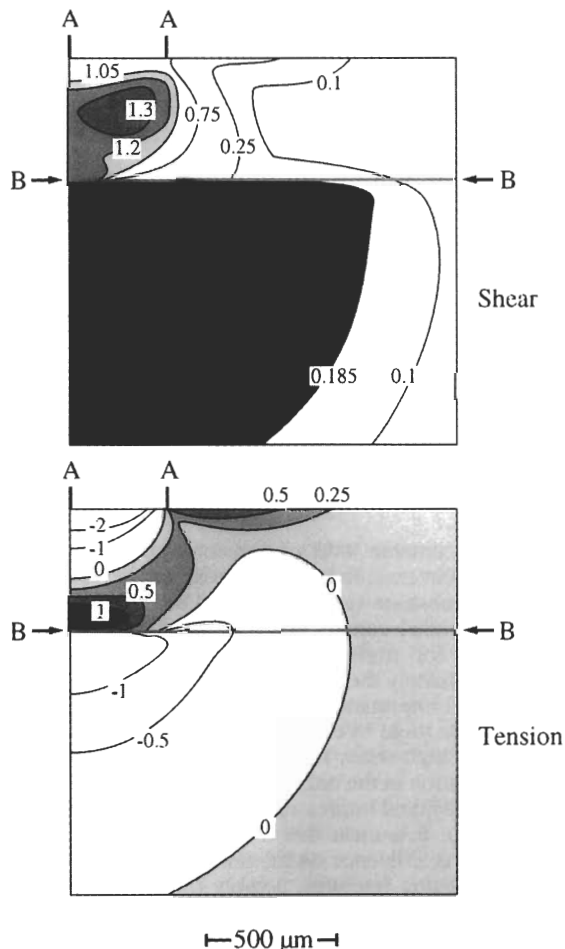


Fig. 7. FEM-computed stress contours for thick-coating Al₂O₃:40 wt% TiO₂/steel system, coating/substrate boundary BB. Indentation with WC sphere, radius *r* = 3.18 mm, load *P* = 1500 N, contact radius AA (cf. Fig. 3). Upper diagram, maximum principal shear stresses, yield zone shaded; lower diagram, maximum principal stresses, tensile zone shaded. Stresses in gigapascals.

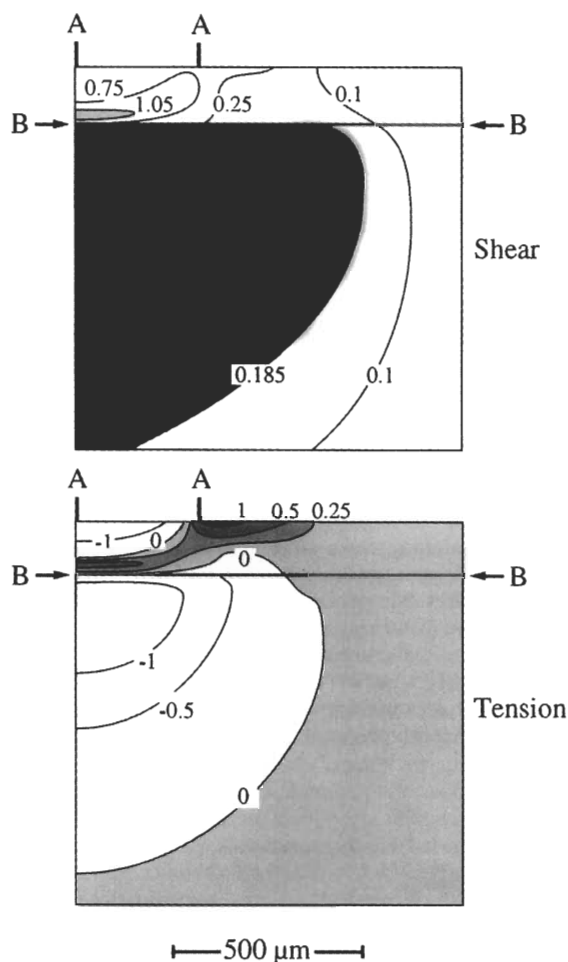


Fig. 8. FEM-computed stress contours for thin-coating Al_2O_3 :40 wt% TiO_2 /steel system, coating/substrate boundary **BB**. Indentation with WC sphere, radius $r = 3.18$ mm, load $P = 500$ N, contact radius **AA** (cf. Fig. 4). Upper diagram, maximum principal shear stresses, yield zone shaded; lower diagram, maximum principal stresses, tensile zone shaded. Stresses in gigapascals.

somewhat less compelling, even allowing for experimental and computational error, perhaps reflecting oversimplification of the nonlinear material response (linear strain hardening), neglect of interactions between plasticity and fracture modes, etc.

Given an acceptable level of agreement between computational and experimental indentation stress-strain results for any given coating/substrate system, the FEM algorithm can be used to map out detailed contact stress fields. This is an essential starting point for understanding the macroscopic damage modes and ultimately the underlying shear fault micromechanisms. Of central importance in the present analysis is the strong role of substrate yield in the composite stress-strain response, notably in the high-strain tail region (Fig. 1). Limited quasi-plastic deformation in the coating is also of interest, accounting for the strong residual impression observed in the coating layer (Figs. 3 and 4). It is clear that these plasticity modes have a major modifying influence on the tensile stress concentrations driving any ensuing fractures, notably the transverse through-thickness cracks (on loading) and delamination cracks (on unloading). That puts us in a position to evaluate the distributions of such tensile stresses, and thence to use fracture mechanics to predict crack behavior.³⁶ As indicated in Section III, any additional residual stresses from thermal expansion mismatch would have to be appropriately superposed onto these stresses.

As already indicated, whereas the choice of plasma-sprayed Al_2O_3 :40 wt% TiO_2 on steel as a model coating/substrate system has an obvious relevance to thermal barrier coatings, the

methodology has application to a much broader range of layer structures. We would reiterate the special facility of FEM to accommodate additional degrees of geometrical complexity. Consideration of thin hard and/or brittle films on soft substrates² is a simple matter of scaling the layer thickness in the FEM code. The approach is not limited to ceramic/metal systems, although the inclusion of at least one ceramic component does open up the possibility of defining new modes of deformation (quasi-plasticity) and fracture (transverse cracks, especially those extending upward from interlayer interfaces). Extension to all-ceramic bilayer systems^{24,25} would appear to be straightforward. In the present Al_2O_3 :40 wt% TiO_2 /steel system, we might consider the addition of an intervening bond coat layer, as is most common in practical thermal barrier coatings. All that would be needed is an independent calibration of the bond coat material, in the manner described herein for the individual Al_2O_3 :40 wt% TiO_2 and steel materials (Section IV). Further extension to multilayer structures with alternating brittle and plastic layers^{26,29} may be envisioned, limited only by computer capacity. Even more complex geometrical laminate configurations, such as those that occur in biosystems (teeth, bone), could conceivably also be handled in this way.

Finally, the Hertzian contact methodology proposed in the present study may be seen as a useful adjunct in the context of material and geometrical design of layer structures. What are the best material combinations, and in what layer thicknesses, for applications with high stress concentrations? Thus, recall the maximum in the layer-structure stress-strain curve in Fig. 1, indicating a transfer in load support from hard coating to soft substrate at high contact loads, with accompanying energy absorption (damage tolerance). Recall also that the maximum increases with coating thickness, but at the expense of a diminishing tail. The most suitable configuration for any prospective contact damage event will then depend on the nature and degree of sustainable damage that can be tolerated, e.g., whether the principal requirement is the capacity to avoid accompanying fracture (bearing applications) or to absorb damage (e.g., armor applications). In the Al_2O_3 :40 wt% TiO_2 /steel system, for instance, the structure shows a remarkable capacity to sustain extensive deformation and fracture damage without failure; herein lies the formula for the practical success of defect-ridden structures like thermal barrier coatings. Material selection criteria for particular applications may therefore call for very specific mismatch conditions, to optimize requisite damage resistance. The Hertzian test, in conjunction with FEM, offers one route to such optimization.

Acknowledgments: We wish to thank C. C. Berndt and G. Bancke at the University of New York, Stony Brook, for supplying the coatings.

References

- H. Herman, "Plasma-Sprayed Coatings," *Sci. Am.*, **256** [9] 113–88 (1988).
- J. C. Knight, T. F. Page, and I. M. Hutchings, "The Influence of Substrate Hardness on the Response of TiN-Coated Steels to Surface Deformation," *Thin Solid Films*, **177**, 117–32 (1989).
- P. Montmitonnet, M. L. Edinger, and E. Felder, "Finite Element Analysis of Elastoplastic Indentation: Part II—Application to Hard Coatings," *J. Tribol.*, **115**, 15–19 (1993).
- H. Herman, C. C. Berndt, and H. Wang, "Plasma-Sprayed Ceramic Coatings"; pp. 131–88 in *Ceramic Films and Coatings*. Edited by J. B. Wachtman and R. A. Haber. Noyes Publications, Park Ridge, NJ, 1993.
- E. H. Lutz, "Microstructure and Properties of Plasma Ceramics," *J. Am. Ceram. Soc.*, **77** [5] 1274–80 (1994).
- A. H. Bartlett and R. D. Maschio, "Failure Mechanisms of a Zirconia-8 wt% Yttria Thermal Barrier Coating," *J. Am. Ceram. Soc.*, **78** [4] 1018–24 (1995).
- A. Pajares, L. Wei, B. R. Lawn, N. P. Padture, and C. C. Berndt, "Mechanical Characterization of Plasma-Sprayed Ceramic Coatings on Metal Substrates by Contact Testing," *Mater. Sci. Eng.*, **A208** [2] 158–65 (1996).
- H. Hertz, *Hertz's Miscellaneous Papers*; Chs. 5 and 6. Macmillan, London, U.K., 1896.
- D. Tabor, *Hardness of Metals*. Clarendon, Oxford, U.K., 1951.
- K. L. Johnson, *Contact Mechanics*. Cambridge University Press, London, U.K., 1985.
- J. S. Field and M. V. Swain, "A Simple Predictive Model for Spherical Indentation," *J. Mater. Res.*, **8**, 297–306 (1993).
- F. C. Roesler, "Brittle Fractures Near Equilibrium," *Proc. Phys. Soc. London*, **B69**, 981 (1956).

- ¹³F. C. Frank and B. R. Lawn, "On the Theory of Hertzian Fracture," *Proc. R. Soc. London*, **A299** [1458] 291-306 (1967).
- ¹⁴B. R. Lawn and T. R. Wilshaw, "Indentation Fracture: Principles and Applications," *J. Mater. Sci.*, **10** [6] 1049-81 (1975).
- ¹⁵B. R. Lawn, *Fracture of Brittle Solids*. Cambridge University Press, Cambridge, U.K., 1993.
- ¹⁶B. R. Lawn, N. P. Padture, H. Cai, and F. Guiberteau, "Making Ceramics 'Ductile'," *Science*, **263**, 1114-16 (1994).
- ¹⁷F. Guiberteau, N. P. Padture, H. Cai, and B. R. Lawn, "Indentation Fatigue: A Simple Cyclic Hertzian Test for Measuring Damage Accumulation in Polycrystalline Ceramics," *Philos. Mag. A*, **68** [5] 1003-16 (1993).
- ¹⁸F. Guiberteau, N. P. Padture, and B. R. Lawn, "Effect of Grain Size on Hertzian Contact in Alumina," *J. Am. Ceram. Soc.*, **77** [7] 1825-31 (1994).
- ¹⁹H. Cai, M. A. Stevens Kalceff, and B. R. Lawn, "Deformation and Fracture of Mica-Containing Glass-Ceramics in Hertzian Contacts," *J. Mater. Res.*, **9**, [3] 762-70 (1994).
- ²⁰N. P. Padture and B. R. Lawn, "Toughness Properties of a Silicon Carbide with an *In-Situ*-Induced Heterogeneous Grain Structure," *J. Am. Ceram. Soc.*, **77** [10] 2518-22 (1994).
- ²¹H. H. K. Xu, L. Wei, N. P. Padture, B. R. Lawn, and R. L. Yeckley, "Effect of Microstructural Coarsening on Hertzian Contact Damage in Silicon Nitride," *J. Mater. Sci.*, **30**, 869-78 (1995).
- ²²A. Pajares, F. Guiberteau, B. R. Lawn, and S. Lathabai, "Hertzian Contact Damage in Magnesia-Partially-Stabilized Zirconia," *J. Am. Ceram. Soc.*, **78** [4] 1083-86 (1995).
- ²³J. C. Jaeger and N. G. W. Cook, *Fundamentals of Rock Mechanics*. Chapman and Hall, London, U.K., 1971.
- ²⁴L. An, H. M. Chan, N. P. Padture, and B. R. Lawn, "Damage-Resistant Alumina-Based Layer Composites," *J. Mater. Res.*, **11** [1] 204-10 (1996).
- ²⁵S. Wuttiaphan, B. R. Lawn, and N. P. Padture, "Crack Suppression in Strongly Bonded Homogeneous/Heterogeneous Laminates: A Study on Glass/Glass-Ceramic Bilayers," *J. Am. Ceram. Soc.*, **79** [3] 634-40 (1996).
- ²⁶H. Liu, B. R. Lawn, and S. M. Hsu, "Hertzian Contact Response of Tailored Silicon Nitride Multilayers," *J. Am. Ceram. Soc.*, **79** [4] 1009-14 (1996).
- ²⁷A. Pajares, L. Wei, B. R. Lawn, and C. C. Berndt, "Contact Damage in Plasma-Sprayed Alumina-Based Coatings," *J. Am. Ceram. Soc.*, **79** [7] 1907-14 (1996).
- ²⁸L. Wei, A. Pajares, and B. R. Lawn, "Effect of Mechanical Damage on Thermal Conduction of Plasma Sprayed Coatings," *J. Mater. Res.*, in press.
- ²⁹M. C. Shaw, D. B. Marshall, M. S. Dadkhah, and A. G. Evans, "Cracking and Damage Mechanisms in Ceramic/Metal Multilayers," *Acta Metall.*, **41** [11] 3311-22 (1993).
- ³⁰K. Komvopoulos, "Elastic-Plastic Finite Element Analysis of Indented Layered Media," *J. Tribol.*, **111**, 430-39 (1989).
- ³¹A. C. Fischer-Cripps and B. R. Lawn, "Stress Analysis of Contact Deformation in Quasi-Plastic Ceramics," *J. Am. Ceram. Soc.*, **79** [10] 2609-18 (1996).
- ³²M. V. Swain and B. R. Lawn, "A Study of Dislocation Arrays at Spherical Indentations in LiF as a Function of Indentation Stress and Strain," *Phys. Status Solidi*, **35** [2] 909-23 (1969).
- ³³M. V. Swain and J. T. Hagan, "Indentation Plasticity and the Ensuing Fracture of Glass," *J. Phys. D*, **9**, 2201-14 (1976).
- ³⁴A. Pajares, L. Wei, B. R. Lawn, and D. B. Marshall, "Damage Accumulation and Cyclic Fatigue in Mg-PSZ at Hertzian Contacts," *J. Mater. Res.*, **10** [10] 2613-25 (1995).
- ³⁵A. C. Fischer-Cripps and B. R. Lawn, "Indentation Stress-Strain Curves for 'Quasi-Ductile Ceramics,'" *Acta Metall.*, **44** [2] 519-27 (1996).
- ³⁶S. Wuttiaphan and B. R. Lawn, "Analysis of Contact Fracture in Brittle Coatings on Soft Substrates"; unpublished work. □